CONF-8910289--7

~~Appendix E~~

BURNING OF A SPHERICAL FUEL DROPLET IN A UNIFORM SUBSONIC FLOWFIELD

CONF-8910289--7

DE93 002224

Kevork Madooglu and Ann R. Karagozian

Mechanical, Aerospace, and Nuclear Engineering Department

University of California, Los Angeles

FG03-88ER13910

Presented at the

Western States Section/The Combustion Institute

1989 Fall Meeting

Sandia National Laboratories

Livermore, California

Paper No. 89-65

BURNING OF A SPHERICAL FUEL DROPLET IN A UNIFORM SUBSONIC FLOWFIELD

Kevork Madooglu and Ann R. Karagozian

Mechanical, Aerospace, and Nuclear Engineering Department

University of California, Los Angeles

ABSTRACT

An analytical/numerical model is described for the evaporation and burning of a spherical fuel droplet in a subsonic crossflow. The external gaseous flowfield is represented using an approximate compressible potential solution, while the internal flowfield of the droplet is represented by the classical Hill's spherical vortex. This allows numerical solution for the external boundary layer and diffusion flame characteristics to be made, from which the droplet's effective drag coefficent, rate of mass loss, size, and flame shape are determined. Comparison with experimental data indicate good agreement, and thus the potential for such simplified models in performing parametric studies.

INTRODUCTION

Over the past few decades, the widespread use of liquid sprays in combustion systems has led to increased research interest in the study of droplet evaporation and combustion in a convective environment, as pointed out in a number of comprehensive review articles [1-3]. Especially in the 1980's, extensive effort has been directed toward the analytical and computational modeling of this problem, which is complicated by the transient, multi-phase, multi-dimensional nature of the transfer processes involved.

Although for most of the droplet lifetime the Reynolds numbers in both gas and liquid phases are not larger than O(100–1000) in many practical combustor situations, Prakash and Sirignano [4] are able to obtain reasonable results with high-Re asymptotics for an evaporating droplet. They solve the gaseous boundary layer with an integral equation approach and couple it to the recirculating liquid flow, placing emphasis on the unsteady liquid-phase heat transfer. Renksizbulut and Yuen [5] and Dwyer and Sanders

[6], on the other hand, treat the same problem by solving the full Navier-Stokes equations numerically. The former authors also report experimental results for freely suspended evaporating drops in hot streams [7]. More recently, Dwyer and Sanders [8] have included chemical reaction in their computations, which provides valuable information on the evaporation and burning processes of droplets at low and intermediate Reynolds numbers, i.e., $Re \leq O(100)$. However, apparently due to the immense computational effort required, these fully-numerical models frequently involve various simplifications in each calculation, such as assuming constant gas properties, neglecting liquid-phase motion and heat transfer, and/or restricting the range of Reynolds and liquid Peclet numbers.

The present study aims at developing an analytical/numerical model for single droplet combustion in a uniform convective flowfield which includes the significant features of the problem without requiring large computational times. Encouraged by the analytical work of Prakash and Sirignano [4], a moderate-to-high Reynolds number model assuming "thin" viscous boundary layers adjacent to the gas-liquid interface is employed here, in which species diffusion and the presence of a diffusion flame are represented. The external, gaseous flowfield about the droplet is solved by an approximate analytical method, and this solution is used to drive the external boundary layer and internal flow of the droplet. A schematic description of the features of the present model is shown in Fig. 1. Another novel feature of the present formulation is that it accounts for the effects of compressibility in the flow approaching the droplet, so that it enables a Mach number-dependent analysis for the gaseous boundary layer which is sufficiently accurate for free stream Mach numbers $M_\infty < 0.3$.

INVISCID FLOW SOLUTIONS

External gaseous flowfield

The external inviscid gas flow about the spherical droplet is represented by a compressible potential flow solution. Defining the velocity potential $\phi(r,\theta)$ for axisymmetric fluid motion, the potential equation for steady, irrotational, isentropic flow of a perfect gas reduces to [9]:

$$\left[1 - \frac{M_\infty^2}{2}(\gamma-1)\left(\mathbf{u}\cdot\mathbf{u} - 1\right)\right]\nabla^2\phi = \frac{M_\infty^2}{2}\left[u_r\frac{\partial}{\partial r} + \frac{u_\theta}{r}\frac{\partial}{\partial\theta}\right]\mathbf{u}\cdot\mathbf{u}. \qquad (1)$$

We note that the isentropic flow assumption requires any chemical reaction to take place within the viscous boundary layer adjacent to the spherical droplet.

The boundary conditions for equation (1) are given by the requirements that the flow is uniform far from the sphere and that the normal velocity at the sphere's surface is zero. For "slightly compressible" flow, i.e. small free-stream Mach number ($M_\infty^2 \ll 1$), the solution of equation (1) can be expanded into the form [9]:

$$\phi(r,\theta;M_\infty^2) = \phi_0(r,\theta) + M_\infty^2\phi_1(r,\theta) + O(M_\infty^4). \tag{2}$$

Since it readily follows from equation (1) that all the effects of compressibility are $O(M_\infty^2)$, the zeroth order term $\phi_0(r,\theta)$ in equation (2) is given by the solution of the homogeneous Laplace equation $\nabla^2\phi_0 = 0$, with the boundary conditions

$$\phi_0 \to -u_\infty r\cos\theta \quad \text{as } r \to \infty, \tag{3a}$$

and

$$\frac{\partial\phi_0}{\partial r} = 0 \quad \text{at } r = R. \tag{3b}$$

This, of course, recovers the well-known solution for incompressible potential flow over a sphere [10]:

$$\phi_0(\hat{r},\theta) = -u_\infty R\left[1 + \frac{1}{2\hat{r}^3}\right]\hat{r}\cos\theta, \tag{4}$$

where a dimensionless radial coordinate is introduced as $\hat{r} = r/R$.

For the first-order term $\phi_1(\hat{r},\theta)$, one has from equations (1) and (2)

$$\nabla^2\phi_1 = \frac{1}{2R^2}\left[\frac{\partial\phi_0}{\partial\hat{r}}\frac{\partial}{\partial\hat{r}} + \frac{1}{\hat{r}^2}\frac{\partial\phi_0}{\partial\theta}\right]\left[\left[\frac{\partial\phi_0}{\partial\hat{r}}\right]^2 + \left[\frac{1}{\hat{r}}\frac{\partial\phi_0}{\partial\theta}\right]^2\right] \tag{5}$$

The boundary conditions for the velocity potential $\phi(\hat{r},\theta)$ have already been satisfied by the zeroth order solution $\phi_0(\hat{r},\theta)$, so that $\phi_1 \to 0$ as $\hat{r} \to \infty$ and $\dfrac{\partial\phi_1}{\partial\hat{r}} = 0$ at $\hat{r} = 1$. Substituting $\phi_0(\hat{r},\theta)$ from (4) into (5), one obtains the explicit governing equation for ϕ_1:

$$\nabla^2\phi_1 = -\frac{u_\infty}{R}\left[\left[\frac{9}{8}\hat{r}^{-4} - \frac{9}{2}\hat{r}^{-7} + \frac{81}{32}\hat{r}^{-10}\right]\cos\theta + \left[\frac{15}{8}\hat{r}^{-4} - \frac{3}{2}\hat{r}^{-7} + \frac{15}{32}\hat{r}^{-10}\right]\cos 3\theta\right]$$

which can be solved by separation of variables, yielding the expression

$$\phi_1(\hat{r},\theta) = -u_\infty R\left[\left[\frac{53}{240}\hat{r}^{-2} + \frac{81}{440}\hat{r}^{-4} - \frac{5}{16}\hat{r}^{-5} + \frac{203}{4224}\hat{r}^{-8}\right]\cos\theta\right]$$

$$+u_\infty R\left[\left(\frac{3}{16}\hat{r}^{-2}-\frac{27}{88}\hat{r}^{-4}+\frac{3}{16}\hat{r}^{-5}-\frac{15}{1408}\hat{r}^{-6}\right)\cos 3\theta\right] \tag{7}$$

The potential-flow solution for the external gas flow is thus obtained to order M_∞^4, which can be regarded as sufficiently accurate for the low subsonic flow regime.

Assuming the viscous layer to be "thin", i.e. the boundary-layer approximation to be valid, the velocity at the edge of the viscous layer, $u_e(\theta)$, is obtained from differentiation of the velocity potential ϕ, which gives

$$\frac{u_e(\theta)}{u_\infty}=\frac{3}{2}\sin\theta-\frac{83}{220}M_\infty^2\sin\theta\left[1-\frac{1215}{664}\sin^2\theta\right]+O(M_\infty^4). \tag{8}$$

For isentropic inviscid flow, the temperature, pressure, and Mach number at the boundary layer edge can be computed from freestream values in a straightforward manner.

Internal liquid flow

The gas flow over a liquid drop induces a liquid-phase motion within the drop through momentum transfer at the gas-liquid interface. Harper and Moore [11] show that the internal recirculating flow of a droplet in a convective environment can be represented by the well-known Hill's spherical vortex solution if one neglects the existence of small counterflow vortices near the downstream stagnation point driven by the vortical flowfield beyond the separation point. In the high Reynolds number limit, the streamsurfaces for this type of flow are described by the stream function

$$\psi=\psi_o-\frac{1}{2}AR^4\hat{r}^2(1-\hat{r}^2)\sin^2\theta\,, \tag{9}$$

and the surfaces of constant vorticity by

$$\omega=5\,AR\,\hat{r}\sin\theta\,. \tag{10}$$

In the above equations, A denotes the vortex strength, which is a constant throughout the inviscid liquid-flow region.

The velocity components of the liquid flow are then

$$u_r=\frac{1}{r^2\sin\theta}\frac{\partial\psi}{\partial\theta}=AR^2(1-\hat{r}^2)\cos\theta$$

and

$$u_\theta = -\frac{1}{r\sin\theta}\frac{\partial\psi}{\partial r} = -AR^2(1-2\tilde{r}^2)\sin\theta\,.$$

As a first approximation, then, the velocity at the edge of an internal viscous layer, $u_i(\theta)$, is represented by the magnitude of the Hill's vortex velocity vector at $r = R$:

$$u_i(\theta) \simeq AR^2 \sin\theta\,, \tag{11}$$

indicating that the presence of the internal viscous layer is actually neglected here. This assumption will be discussed in detail in the Results section. The unknown vortex strength A is to be determined through the coupling of the gaseous and liquid-phase solutions.

GASEOUS BOUNDARY LAYER ANALYSIS

For the viscous gas flow adjacent to the droplet surface, the governing equations and boundary conditions account for the effects of chemical reaction, tangential surface motion, and mass blowing due to evaporation (and combustion) at the gas-liquid interface within the framework of a laminar axisymmetric boundary layer. The burning process is represented at present by infinitely fast reaction kinetics, which shrinks the reaction zone effectively into a "flame sheet" of zero thickness within the boundary layer, dividing it into two regions (see Fig. 2). The governing equations, written in surface coordinates (x,y), are then

$$\frac{\partial}{\partial x}(r_s\rho u) + \frac{\partial}{\partial y}(r_s\rho v) = 0\,, \tag{12}$$

$$\rho\left[u\frac{\partial u}{\partial x} + v\frac{\partial u}{\partial y}\right] = \rho_e u_e\frac{du_e}{dx} + \frac{\partial}{\partial y}\left[\mu\frac{\partial u}{\partial y}\right], \tag{13}$$

and

$$\rho\left[u\frac{\partial H}{\partial x} + v\frac{\partial H}{\partial y}\right] = \frac{\partial}{\partial y}\left[\frac{\mu}{Pr}\frac{\partial H}{\partial y}\right] + \frac{\partial}{\partial y}\left[\frac{\mu}{Pr}(Pr-1)\frac{\partial}{\partial y}\left[\frac{u^2}{2}\right]\right] - qm_f\,, \tag{14}$$

where $r_s(x)$ is the radius of the cross-section of the sphere at x.

The equations for conservation of species take the form

$$\text{Region I, } y \le y_f\text{:}\quad \rho\left[u\frac{\partial K_f}{\partial x} + v\frac{\partial K_f}{\partial y}\right] = \frac{\partial}{\partial y}\left[\rho D\frac{\partial K_f}{\partial y}\right] + m_f\,, \tag{15a}$$

$$K_p = 1 - K_f\,, \tag{15b}$$

$$\text{Region II, } y \geq y_f: \quad \rho\left[u\frac{\partial K_o}{\partial x} + v\frac{\partial K_o}{\partial y}\right] = \frac{\partial}{\partial y}\left[\rho D\frac{\partial K_o}{\partial y}\right] + \frac{1}{f^*}m_f\,, \tag{16a}$$

$$K_p = 1 - K_o\,. \tag{16b}$$

Here f^* is the stoichiometric fuel-oxidizer mass-consumption ratio, given by

$$f^* = \frac{-(\partial K_f/\partial y)_{y_f}}{(\partial K_o/\partial y)_{y_f}}\,.$$

All inert gases are assumed to have the same properties as the products of reaction and are treated together with the latter as one species. Furthermore, in the above equations, the simplifying assumption has been made that all the species involved in the problem have the same diffusion coefficient D.

The presence of a flame sheet in the boundary layer introduces discontinuities in the enthalpy and concentration gradients at this location. Defining new composite variables for enthalpy and mass fraction,

$$G \equiv \frac{H + f^*qK_o}{H_e + f^*qK_{o,e}} \tag{17a}$$

and

$$K \equiv K_o - \frac{1}{f^*}K_f, \tag{17b}$$

these discontinuities as well as the source terms in equations (14), (15a) and (16a) are eliminated [12,13]. For laminar, axisymmetric boundary layer flows with variable gas properties, Lees (1956) suggests the following coordinate transformation that incorporates elements of the Mangler, Howarth-Dorodnitsyn and Levy transformations [14]:

$$\xi(x) = \int_0^x \rho_e\mu_e u_e r_s^2 dx \tag{18}$$

and

$$\eta(x,y) = \frac{u_e r_s}{(2\xi)^{1/2}}\int_0^y \rho dy \tag{19}$$

Then defining a non-dimensional compressible stream function

$$f \equiv \frac{\Psi(x,y)}{(2\xi)^{1/2}} \tag{20}$$

where

$$\frac{\partial \Psi}{\partial y} = r_s \rho u, \qquad \frac{\partial \Psi}{\partial x} = -r_s \rho v,$$

the original governing equations can be transformed into a set of ordinary differential equations, provided that there exist locally self-similar solutions, i.e. if f, G and K are functions of η only. Thus finally introducing the non-dimensional velocity

$$F(\eta) \equiv \frac{df}{d\eta} = \frac{u}{u_e}, \tag{21}$$

one then obtains the governing equations for $\rho\mu$ = const. and unity Lewis number,

$$F''(\eta) + f(\eta)F'(\eta) - \beta(\xi)\left[\frac{\rho_e}{\rho} - F^2(\eta)\right] = 0, \tag{22a}$$

$$G''(\eta) + Pr\, f(\eta)G'(\eta) = (1-Pr)\frac{u_e^2}{g_e}\left[F(\eta)F''(\eta) + F'^2(\eta)\right], \tag{22b}$$

$$K''(\eta) + Sc\, f(\eta)K'(\eta) = 0, \tag{22c}$$

where primes denote differentiation with respect to the similarity parameter η. The problem is thus transformed effectively into the well-known wedge-boundary-layer problem, with varying pressure gradients for varying angular positions. The "pressure gradient parameter" $\beta(\xi)$ in equation (22a) is defined as

$$\beta(\xi) = \frac{2\xi}{u_e}\frac{du_e}{d\xi}. \tag{23}$$

Since, at any location x, the pressure is constant across the boundary layer, the density ratio that appears in equation (22a), ρ_e/ρ, is equal to T/T_e, and can be written as

$$\frac{\rho_e}{\rho} = \frac{c_{p,e}}{c_p}\left[\left[1 + \frac{\gamma-1}{2}M_e^2 + Q_e K_{o,e}\right]G(\eta) - \frac{\gamma-1}{2}M_e^2 F^2(\eta)\right] \tag{24a}$$

for $\eta \le \eta_f$, and

$$\frac{\rho_e}{\rho} = \frac{c_{p,e}}{c_p}\left[\left[1 + \frac{\gamma-1}{2}M_e^2 + Q_e K_{o,e}\right]G(\eta) - \frac{\gamma-1}{2}M_e^2 F^2(\eta) - Q_e K(\eta)\right] \tag{24b}$$

for $\eta \ge \eta_f$, where $Q_e \equiv f^* q/(c_{p,e} T_e)$.

The solution of the set of ordinary differential equations (22) is complicated by the fact that the

tangential and normal (blowing) velocities, temperature and species mass fractions at the surface are all unknown as yet. The tangential velocity at the surface, $u_s(x)$, as well as the surface temperature $T_s(x)$ are obtained by coupling the gas-phase flow to the liquid-phase motion through shear-stress continuity and heat transfer relations across the interface, respectively. Two additional relations are required to determine the fuel mass fraction and the mass blowing rate at the surface, and these are provided by the Clausius-Clapeyron equation for equilibrium evaporation and by the condition that the net flux of products through the interface must be zero. The latter implies that

$$\rho_s v_s (1 - K_{f,s}) + \rho_s D_s \left[\frac{\partial K_f}{\partial y}\right]_s = 0 ,$$

which, recalling the definitions of $K(\eta)$ and $f(\eta)$, reduces to

$$K(0) = -\frac{1}{f^*} - \frac{1}{Pr}\frac{K'(0)}{f(0)} . \tag{25}$$

The Clausius-Clapeyron equation provides an equation for the fuel partial pressure at the surface, $P_{f,s}$, in relation to the surface temperature T_s, and some reference state, indicated by the subscript ref:

$$\ln\left[\frac{P_{f,s}}{P_{ref}}\right] = \frac{h_v}{R_f}\left[\frac{1}{T_{ref}} - \frac{1}{T_s}\right] \tag{26}$$

The fuel mass fraction at the surface, $K_{f,s}$, is then related to $P_{f,s}$ through the molecular weights of the fuel and the reaction products.

Both pressure and shear stress at the surface contribute to the drag force D exerted on the droplet by the convective stream. The drag coefficient $C_D \equiv 2D/(\pi R^2 \rho_\infty u_\infty^2)$ is thus computed from the pressure distribution determined from the external flow solution and from the shear stress distribution determined from the boundary layer solution. Since the boundary layer model described in this section does not allow for calculations beyond the separation point θ_s, average quantities are employed to account for the pressure contributions in the region $\theta_s \le \theta \le \pi$. Both measurements and numerical calculations of the pressure distribution on the surface of a sphere in the Reynolds number range of interest, as outlined by Clift, et al. [15], indicate that a constant pressure at half that of the separation point value is a reasonable approximation for the pressure distribution in the region between the separation point and the rearward stagnation point. The surface shear stress in this region is neglected with respect to its contribution to the total drag.

Finally, the total mass transfer, i.e., the rate of evaporation from the droplet, $\dot{m}$, is given by

$$\dot{m} = \int_0^{\pi} (\rho_s v_s)(2\pi R^2 \sin\theta \, d\theta) \, . \tag{27}$$

For the present set of calculations, the contribution of the region beyond the separation point to the overall evaporation rate is neglected. As noted by Prakash and Sirignano [4], and as will be shown below, the rate of mass transfer in the region of the flow beyond the separation point is relatively small. The results presented here can thus be regarded as a lower estimate in terms of convective droplet evaporation.

RESULTS

The set of coupled ordinary differential equations (22) is solved numerically by central differencing at discrete angular positions along the droplet surface until separation is reached. Time-dependent calculations are performed by updating the Reynolds number through the calculated values of evaporation rate and drag at each time step. The dimensionless time scale τ used in these calculations is based on the free stream gas properties and the initial droplet radius, i.e., $\tau = \alpha_\infty / R_0^2$. Here α_∞ denotes the thermal diffusivity of the freestream gas.

In the present calculations, a uniform liquid-phase temperature is assumed. Since earlier work such as that of Prakash and Sirignano [4] has shown that the liquid-phase heating is essentially unsteady in the very early periods of droplet lifetime, calculations presented in this paper would apply to larger droplets in the later stages of evaporation and burning, when a uniform liquid temperature is reached. In the analysis of Harper and Moore [11], the velocity at the surface is taken to be only a small perturbation of its value at the edge of the viscous liquid layer. Prakash and Sirignano [16] show that this is a valid assumption while the same may not be true for vorticity, since the difference in vorticity between the surface and the edge of the viscous layer may not be negligible. However, as seen in Figs. 3 and 4, the overall effect of liquid motion on the transfer processes in the gaseous boundary layer is relatively insignificant. Thus, the emphasis being placed on overall evaporation and drag calculations within the scope of the present study, the surface motion is approximated by the inviscid inner flow solution at the limit $r = R$. This reduces the required computational time for the solution of the coupled gas-liquid boundary layers considerably, since the (presently neglected) liquid boundary layer solution is effectively obtained from calculation of one

unknown parameter, namely the vortex strength A that appears in the boundary conditions for the gas flow. For the case of the burning droplet, where the existence of an envelope flame is assumed a priori, the position of the flame before separation can be calculated. The experimental results of Gollahalli and Brzustowski [17] indicate that the assumption of an envelope flame is realistic for $Re_\infty < 200$.

The present model has been utilized to obtain results for both low and high pressure environments. Calculated temperature, velocity, and species concentration profiles in the boundary layer for specific freestream conditions are shown in Fig. 3. The profiles in this figure indicate that the influence of the internal flowfield of the droplet, which is of the order of 5% of the flow magnitude at the boundary layer edge, is small. While the profiles shown in Fig. 3 correspond to a point 60° from the stagnation point of the droplet, similar behavior is noted at other locations along the droplet surface. This observation is in fact corroborated in Fig. 4, in which the local dimensionless "blowing" velocity component and friction coefficient are plotted as a function of angular distance along the droplet surface. Again, the influence of the internal vortical flowfield is relatively small, although the increase in mass blowing and decrease in shear stress with surface flow is appropriate. This figure also indicates, as noted above, that as the point of separation is approached, the local mass transfer rate becomes very small. Hence neglect of the mass transfer beyond the separation point appears to be reasonable.

It is also noted that the effect of Mach number on droplet evaporative and burning processes is not strong; this is indicated in Fig. 5. As is physically reasonable, the local shear stress near the top of the droplet surface is slightly increased with higher freestream Mach number, but this effect is negligible closer to the stagnation point. The effect of Mach number on mass loss appears to be negligible at all locations along the droplet, although in the absence of the flame (evaporation only), the increased temperature and pressure at the stagnation point with higher M_∞ does slightly increase the mass transfer in that region. It is likely, however, that for higher subsonic crossflows, compressibility effects will be more significant.

The computed variation in drag coefficient for evaporating and burning droplets is shown in Fig. 6, which also provides comparison with the experimental results of Yuen and Chen [18] for an evaporating droplet, and with the "standard curve" for the drag coefficient of a solid sphere. Our calculations appear to correspond well to experimental observations, and indicate the significant influence of mass blowing on the

behavior of the drag coefficient. The calculated rate of mass loss as a function of Reynolds number is shown in Figs. 7ab, for both evaporating and burning droplets at different freestream conditions. The choice of fuel, free-stream, and initial conditions for the case in 7a allows for a direct comparison with the experimental data of Renksizbulut and Yuen [7] for the evaporation rate from a suspended droplet in a hot stream. At a much higher freestream pressure (Fig. 7b), the rate of mass loss for both evaporating and burning droplets is significantly increased. We note here that most other experimental observations on evaporating and burning droplets in a convective environment always involve highly scattered data. In this context, the measurements of Eisenklam, et al. [19] and Natarajan and Brzustowski [20] can also be referenced, although these are at higher pressures. The empirical correlations given in both of these papers result in evaporation rates that are somewhat higher that those reported in [7] as well as those calculated presently. As noted by Dwyer and Sanders [6], this discrepancy could be due to differences in specific mechanisms present (perhaps initial transient droplet heating) which affect the mass transfer.

Figure 8 displays results for the variation in droplet radius and Reynolds number with dimensionless time, τ, with comparison to the experimental observations of Renksizbulut and Yuen [7]. The initial Reynolds number is chosen to be 200, and the initial droplet radius 1 mm. The drag coefficient used to extrapolate the experimental values is taken from the data of Yuen and Chen [18]. Finally, predicted flame shapes, based on local maxima in boundary layer temperature (and the local vanishing in the reactant mass fractions) are shown in Fig. 9 for two different Reynolds numbers. It should be noted that the flame shapes shown are each relative to the instantaneous droplet radius $R(\tau)$. Separation of the flame from the region near the droplet surface appears to coincide with separation of the external boundary layer.

CONCLUSIONS

The present modeling effort demonstrates that, by including only the crucial physical phenomena associated with fuel droplet vaporization and burning in a convective environment, a very reasonable representation for droplet behavior can be obtained. By using analytical representations of the inviscid gas and liquid internal flowfields, and by employing the boundary layer type of assumptions first used by Prakash and Sirignano [4], it is possible to solve for the characteristics of the reacting flow adjacent to the droplet surface. These characteristics allow calculation of parameters which describe droplet evaporation

and burning (drag coefficient, mass transfer rates, size histories) that compare very well with experimental data [7,18]. As noted above, the relatively large amount of scatter present in the experimental data available for burning droplets [19,20] renders comparison with the present model less precise. It should be noted, however, that our predictions lie well within the error bars of the experimental data, but our calculations tend to slightly underpredict (compared with the average of the data) the degree of mass loss by the droplet. Our predictions for mass loss are also somewhat lower than the full- scale numerical predictions made by Dwyer and Sanders [8], but this may be due to the fact that these researchers choose to linearize the exponential term in the Clausius-Clapeyron relation. Despite these minor discrepancies, our model appears to be relatively robust and accurate, with a minimum in required computational times, and thus allows detailed parametric studies to be performed with ease.

NOMENCLATURE

A	Hill's vortex strength
c_p	Specific heat at constant pressure for gas
D	Mass diffusivity
f^s	Stoichiometric fuel-oxidizer ratio
H	Total enthalpy
h_v	Latent heat of vaporization
M	Mach number
$\dot{m}$	Rate of evaporation of droplet
m_f	Mass rate of fuel consumption at the flame
Pr	Prandtl number ($\equiv \mu/(\rho\alpha)$)
q	Heat release per unit mass of fuel
r	Radial coordinate
R	Droplet radius

R_f	Gas constant for fuel vapor
R_o	Initial droplet radius
r_s	Local radius of droplet cross-section
Sc	Schmidt number ($= \mu/(\rho D)$)
T	Temperature
(u_r, u_θ)	r- and θ-components of velocity vector u
(u, v)	Velocity components tangential and normal to droplet surface
(x, y)	Coordinates tangential and normal to droplet surface
y_f	Local flame position relative to droplet surface
α_∞	Thermal diffusivity of freestream gas
β	Pressure gradient parameter
γ	Ratio of specific heats
(η, ξ)	Similarity variables
θ	Coordinate indicating angular distance along droplet
θ_s	Separation point
μ	Dynamic viscosity
ρ	Density
τ	Dimensionless diffusion time scale
ϕ	Velocity potential
ψ	Stream function

Subscripts

e	Conditions at edge of external boundary layer
f	Fuel

i	Conditions associated with internal liquid flowfield
o	Oxidizer
p	Products
ref.	Reference state
s	Liquid surface
∞	Freestream gas conditions

ACKNOWLEDGEMENT

This work is supported by the U.S. Department of Energy, Office of Basic Energy Sciences, Grant No. DE-FG03-88-ER13910.

REFERENCES

1. Law, C.K.: *Progress in Energy and Combustion Science, 8*, 171 (1982).

2. Faeth, G.M.: *Progress in Energy and Combustion Science, 9*, 1 (1983).

3. Sirignano, W.A.: *Progress in Energy and Combustion Science, 9*, 291 (1983).

4. Prakash, S. and W.A. Sirignano: *International Journal of Heat and Mass Transfer, 23*, 253 (1980).

5. Renksizbulut, M. and M.C. Yuen: *ASME Journal of Heat Transfer, 105*, 389 (1983a).

6. Dwyer, H.A. and B.R. Sanders: *Proc. of ASME/JSME Thermal Engineering Joint Conference, 1*, 3 (1987).

7. Renksizbulut, M. and M.C. Yuen: *ASME Journal of Heat Transfer, 105*, 384 (1983b).

8. Dwyer, H.A. and B.R. Sanders: *Twenty-first Symposium (International) on Combustion*, 633 (1986).

9. Van Dyke, M.: *Perturbation Methods in Fluid Mechanics*, Annotated Edition, p. 15, Parabolic Press, Stanford, California, 1975.

10. Panton, R.L.: *Incompressible Flow*, p. 544, John Wiley & Sons, New York, 1984.

11. Harper, J.F. and D.W. Moore: *Journal of Fluid Mechanics, 32*, 367 (1968).

12. Burke, S.P. and T.E.W. Schumann: *Industrial and Engineering Chemistry, 20,* 998 (1928).

13. Chen, T.N. and T.Y. Toong: *Progress in Astronautics and Aeronautics: Heterogeneous Combustion* (H.G. Wolfhard, I. Glassman, L. Green, Eds.), Vol. 15, p. 643, Academic Press, New York, 1964.

14. Lees, L.: *Jet Propulsion, 26,* 259 (1956).

15. Clift, R., J.R. Grace and M.E. Weber: *Bubbles, Drops and Particles,* pp. 108, 129, Academic Press, New York, 1978.

16. Prakash, S. and W.A. Sirignano: *International Journal of Heat and Mass Transfer, 21,* 885 (1978).

17. Gollahalli, S.R. and T.A. Brzustowski: *Fourteenth Symposium (International) on Combustion,* 1333 (1972).

18. Yuen, M.C. and L.W. Chen: *Combustion Science and Technology, 14,* 147 (1976).

19. Eisenklam, P., S.A. Arunchalam and J.A. Weston: *Eleventh Symposium (International) on Combustion,* 715 (1966).

20. Natarajan, R. and T.A. Brzustowski: *Combustion Science and Technology, 2,* 259 (1970).

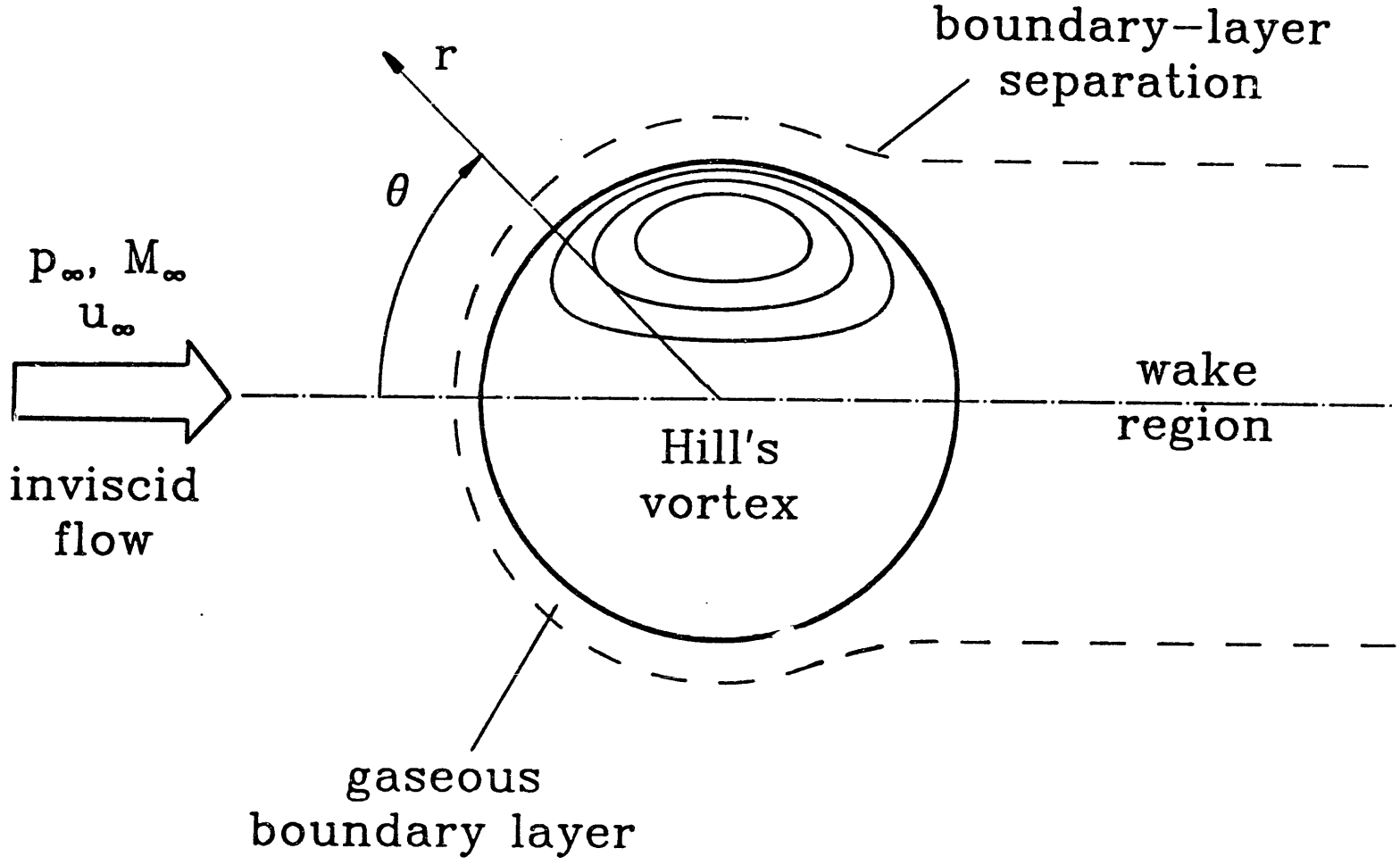

Figure 1. Schematic diagram of the flowfield associated with a liquid fuel droplet in a convective environment.

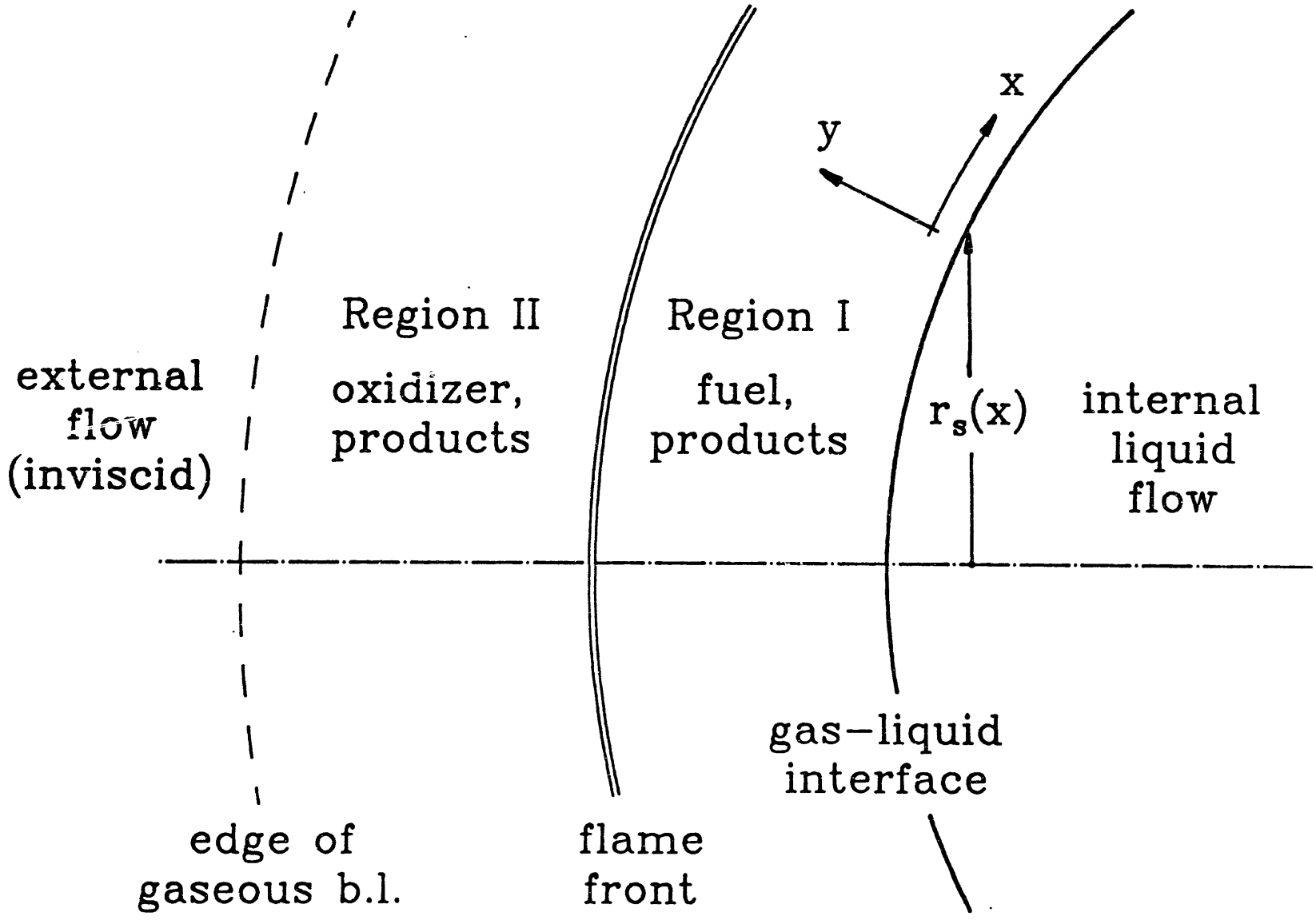

Figure 2. Characteristics of the boundary layer and reaction zone near the surface of the liquid droplet.

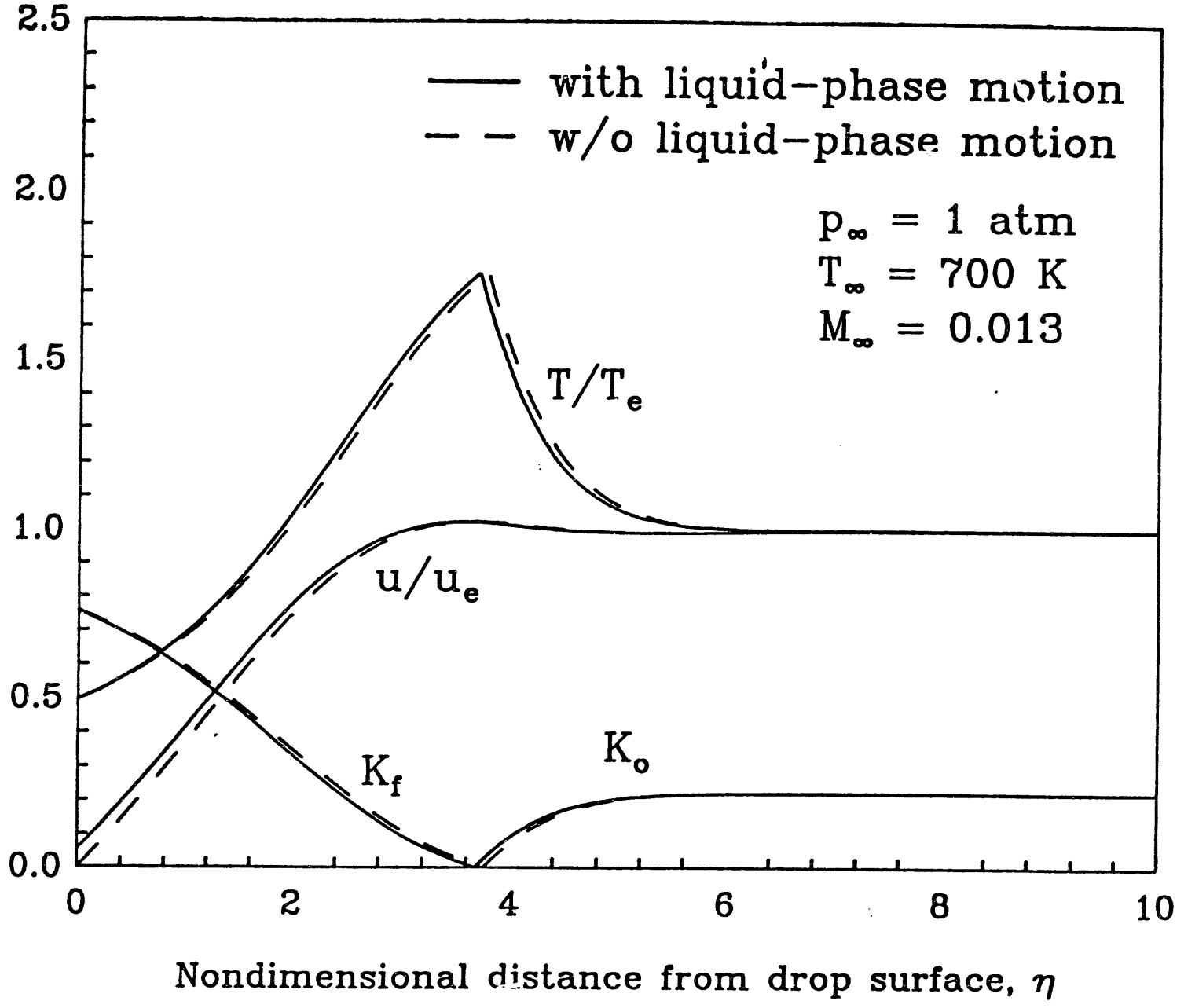

Figure 3. Predicted velocity, temperature, and concentration profiles in the boundary layer of the burning droplet at an angular location $\theta = 60°$ from the stagnation point.

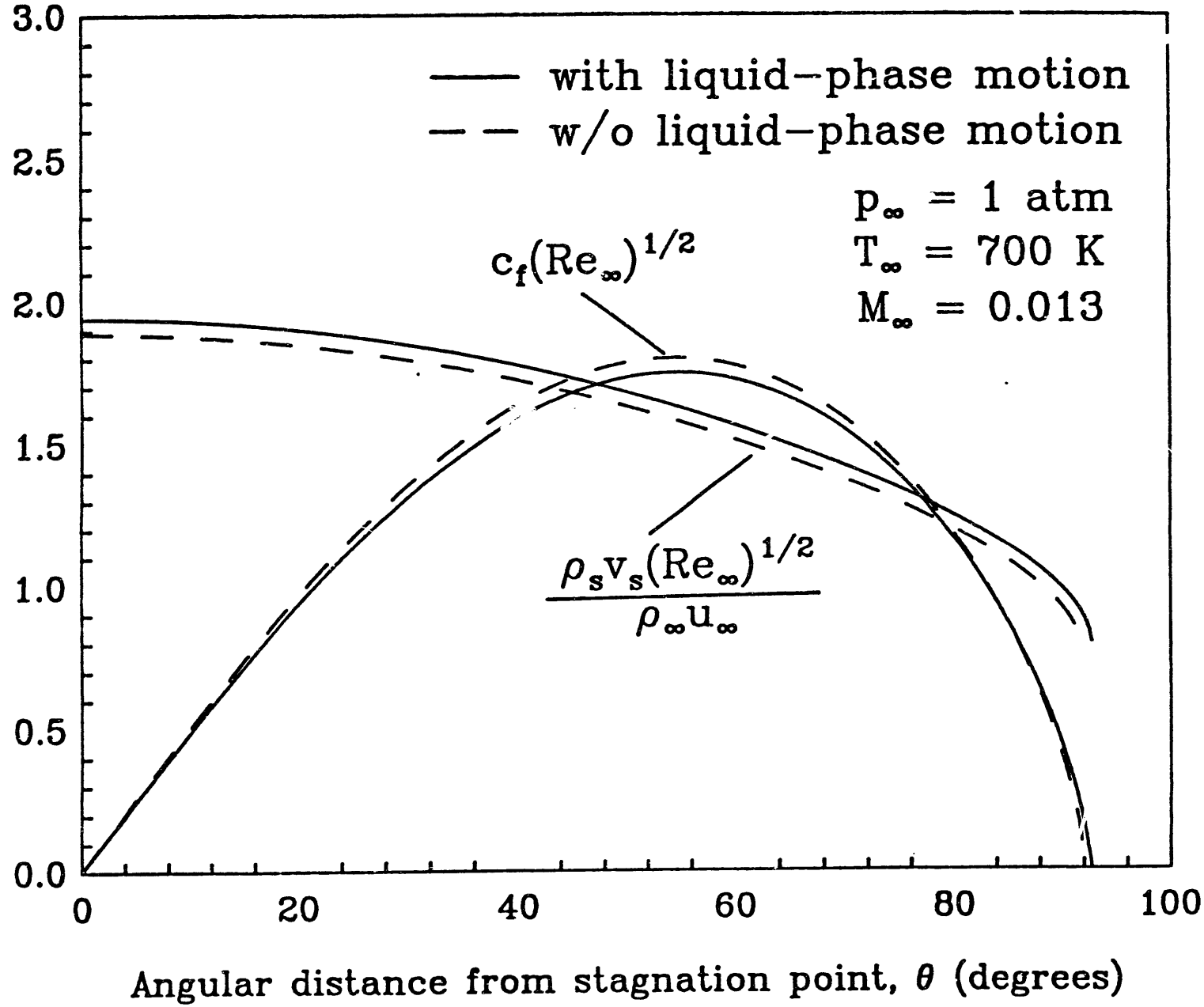

Figure 4. Variation in the skin friction coefficient and evaporation rate per unit area along the burning droplet surface (θ measured from the stagnation point), for the cases with and without surface flow.

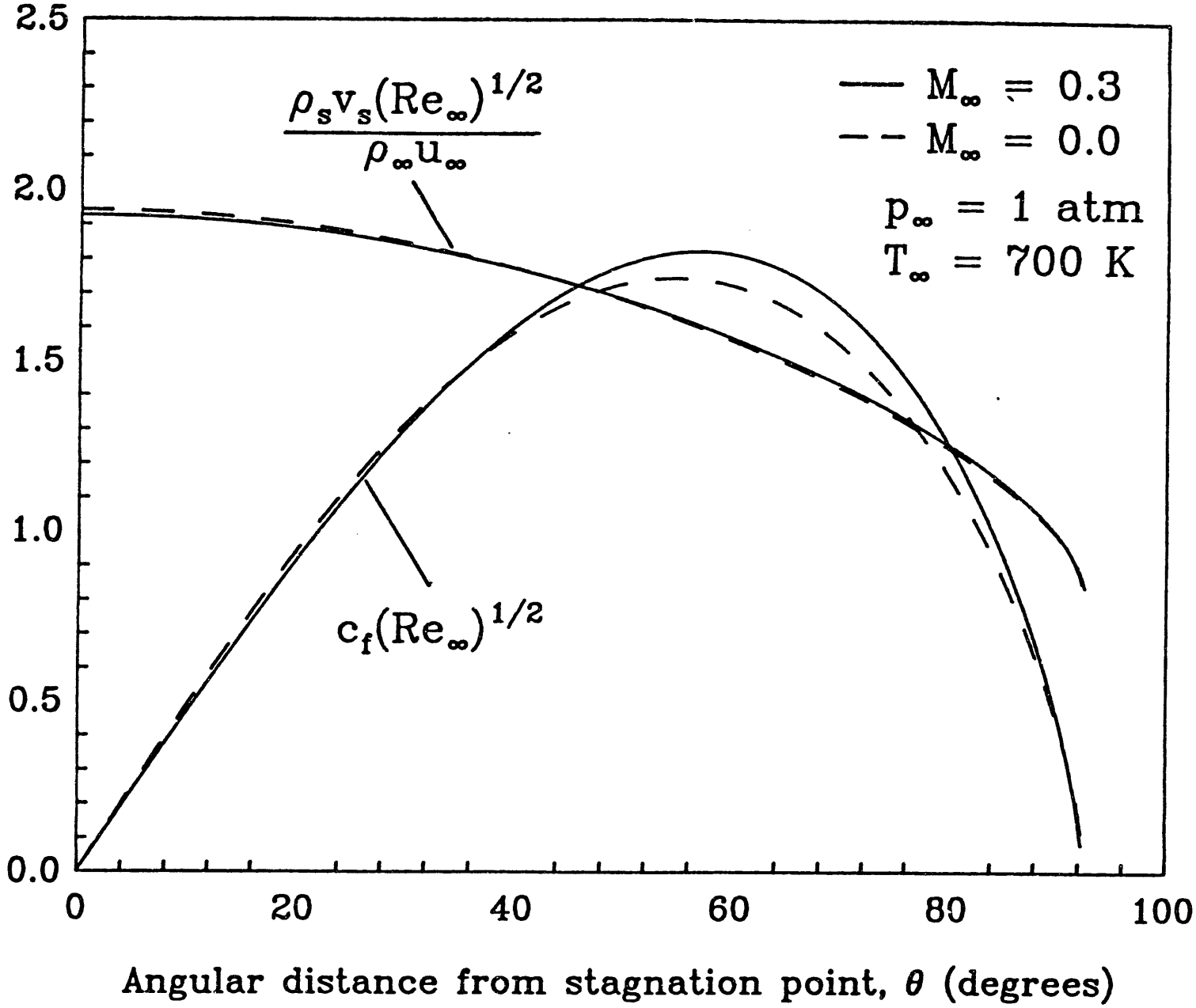

Figure 5. Variation in the skin friction coefficient and evaporation rate per unit area along the burning droplet surface (θ measured from the stagnation point), for the incompressible case and $M_\infty = 0.3$.

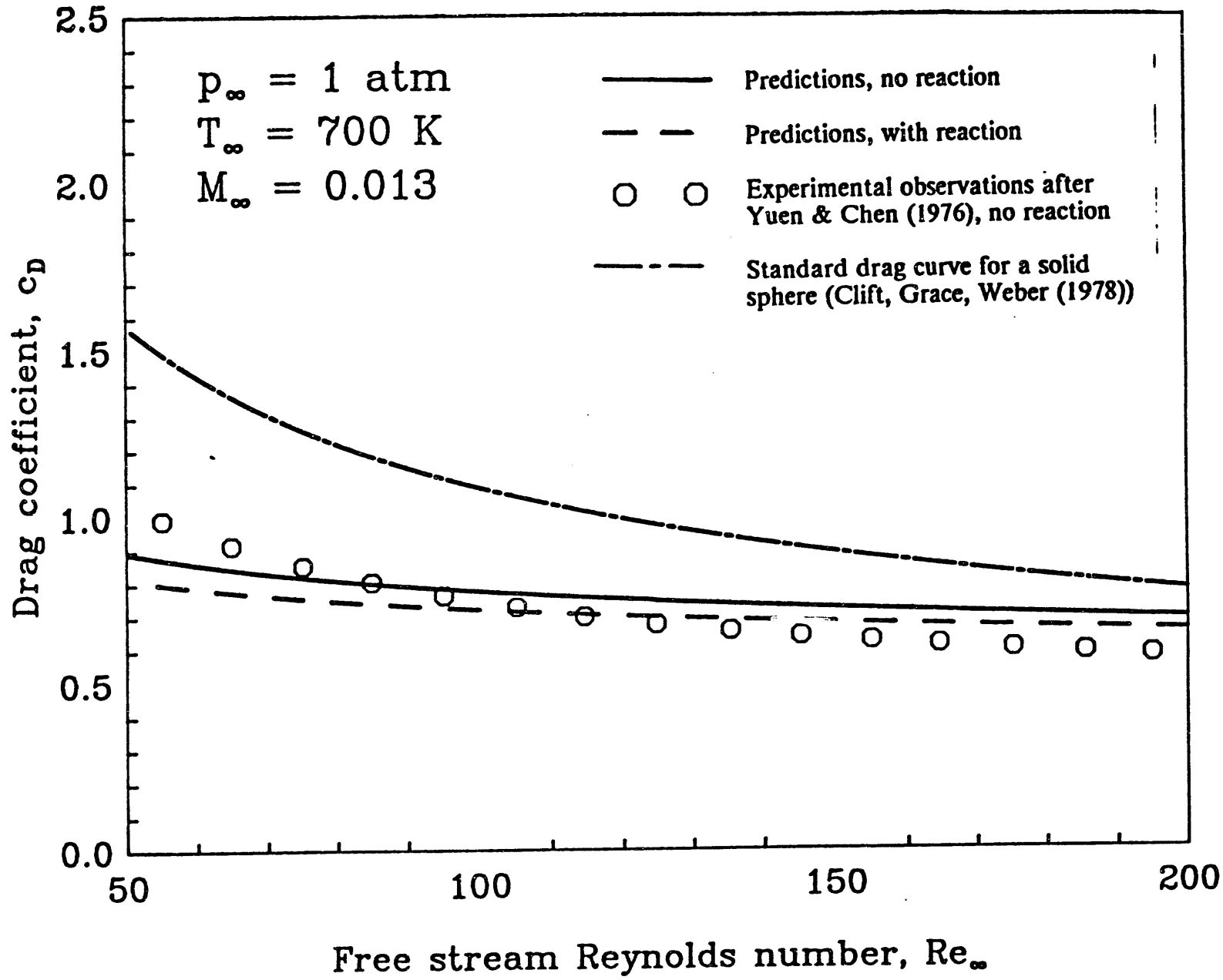

Figure 6. Predicted variation in drag coefficient of the droplet with freestream Reynolds number, for both evaporating and burning droplets. Comparison is made with the experimental data of Yuen and Chen [18]

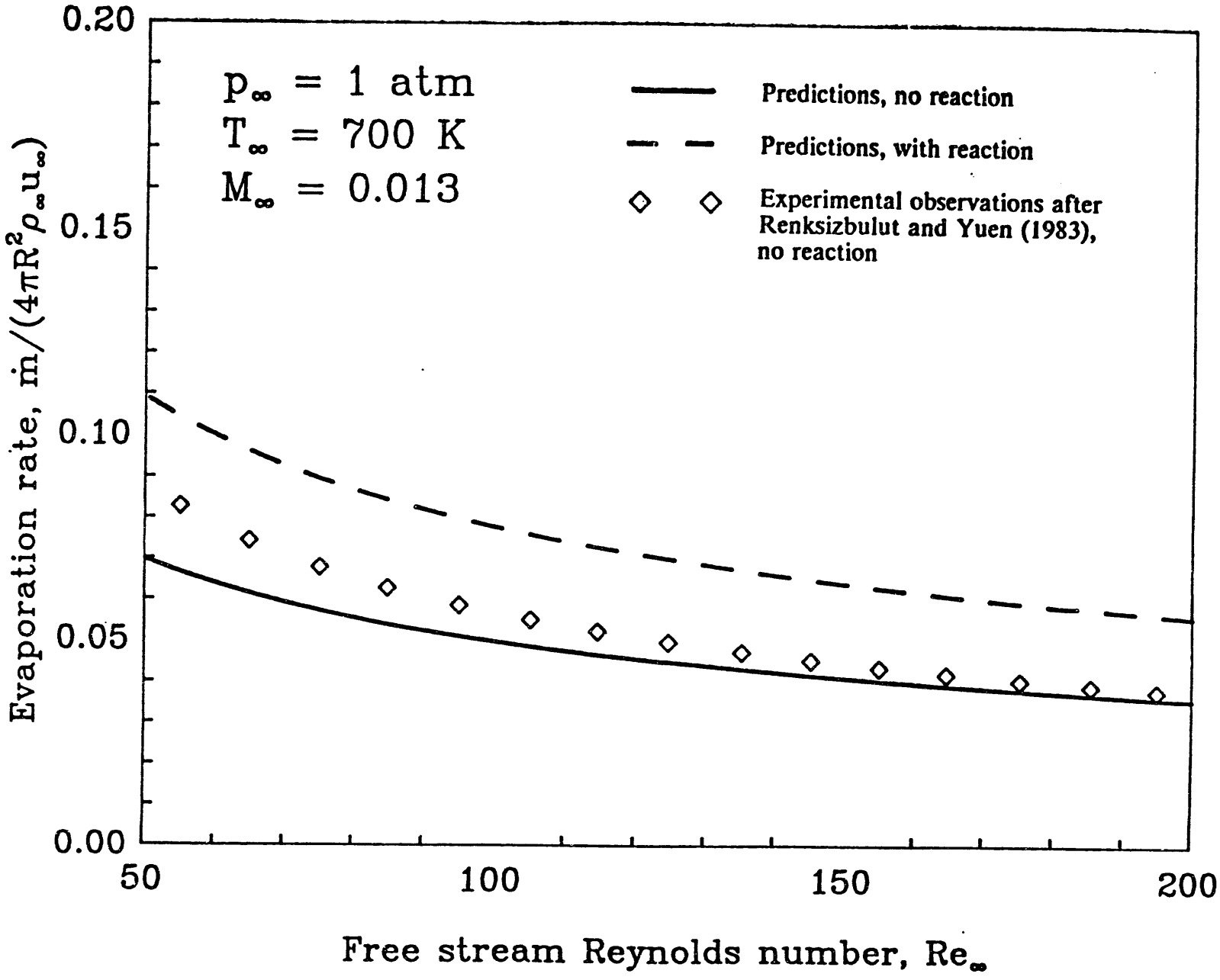

Figure 7a. Predicted variation in mass transfer rate of the droplet with Reynolds number, for evaporating and burning droplets in a low pressure environment. Comparison is made with the experimental data of Renksizbulut and Yuen [7] for an evaporating droplet.

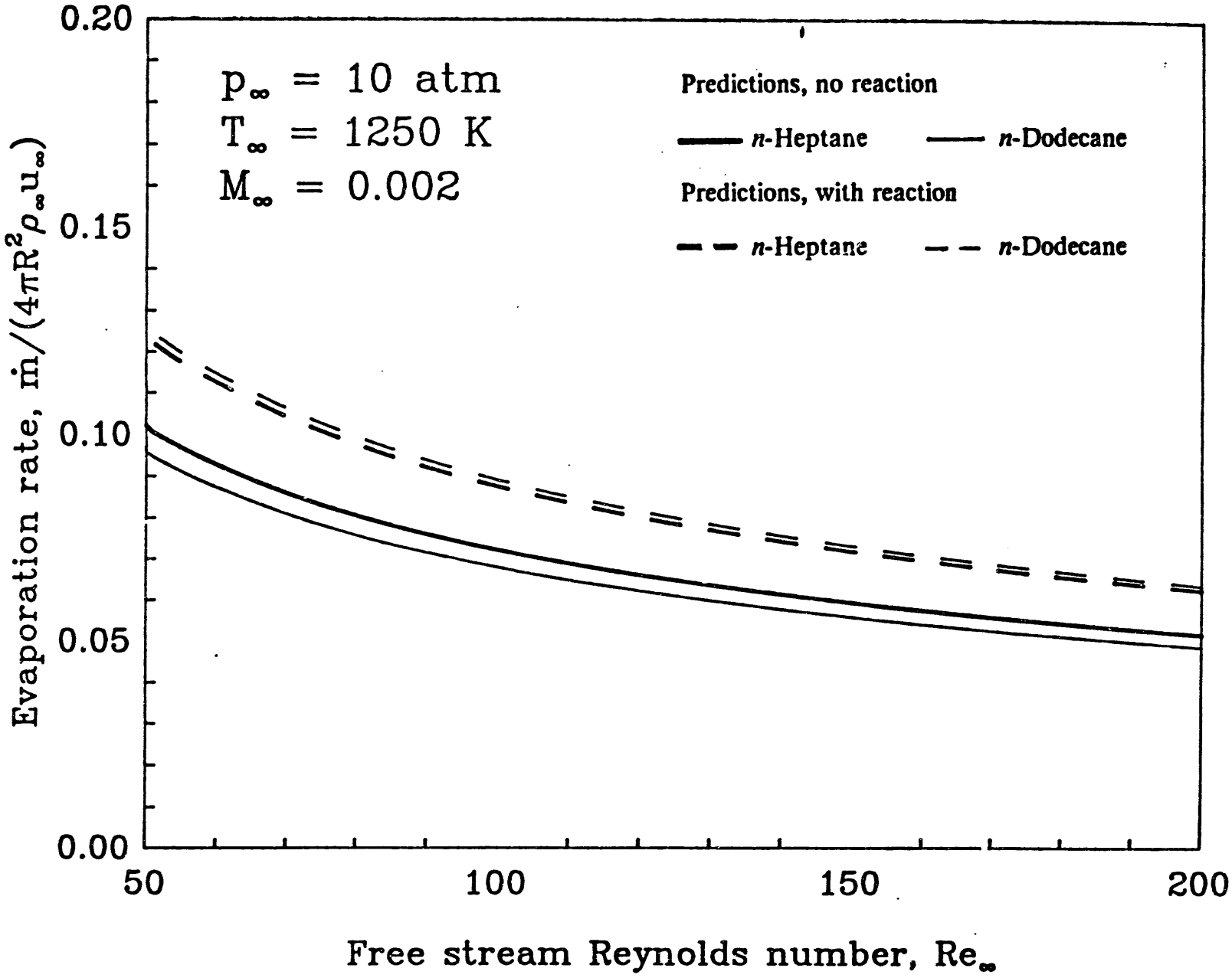

Figure 7b. Predicted variation in mass transfer rate of the droplet with Reynolds number, for evaporating and burning droplets in a high pressure environment. Predictions for both n-Heptane and n-Dodecane are

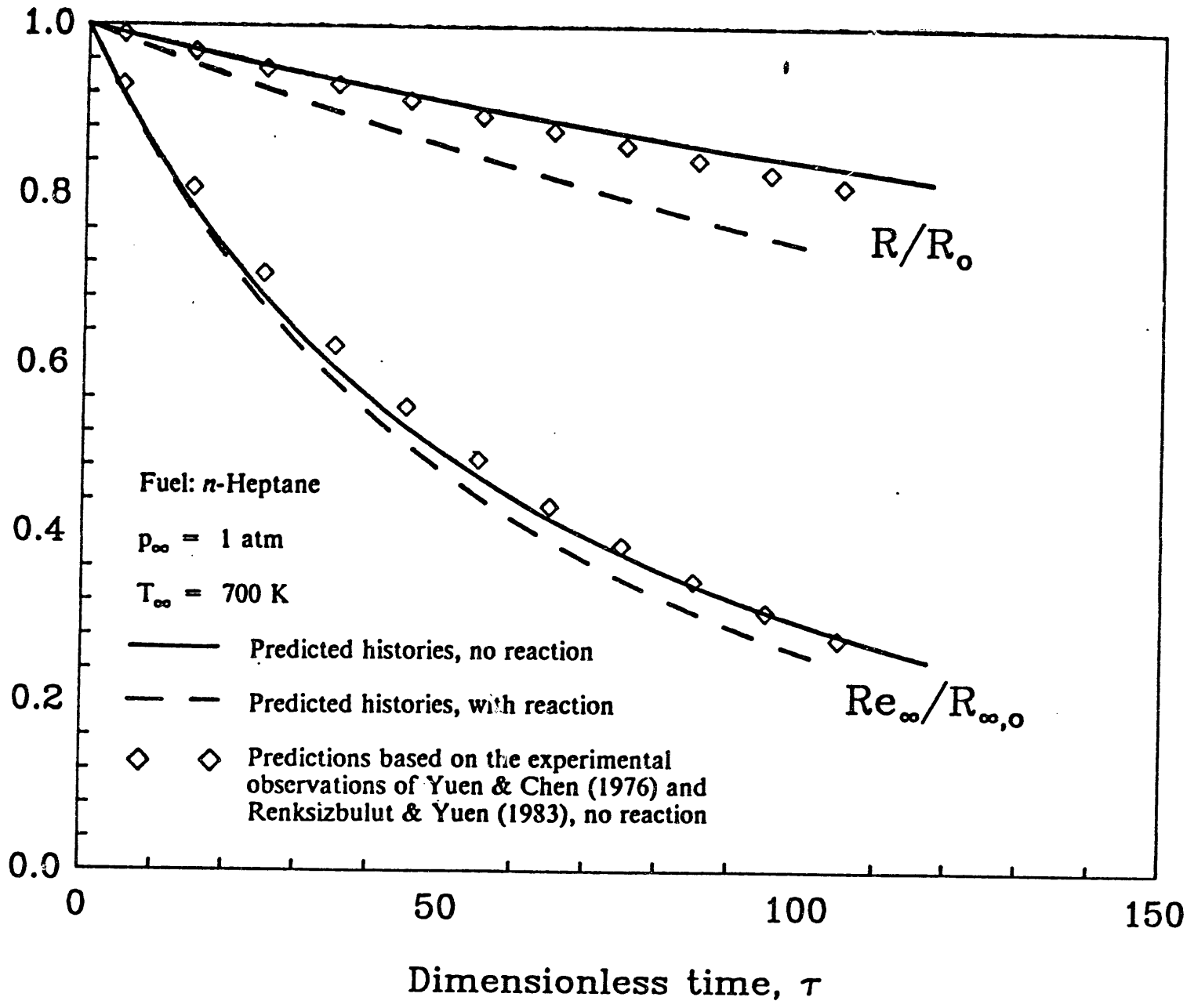

Figure 8. Predicted droplet histories (radius and effective Reynolds number), for evaporating and burning droplets. Comparison is made with the experimental data of Renksizbulut and Yuen [7], using the data on drag coefficient from Yuen and Chen [18].

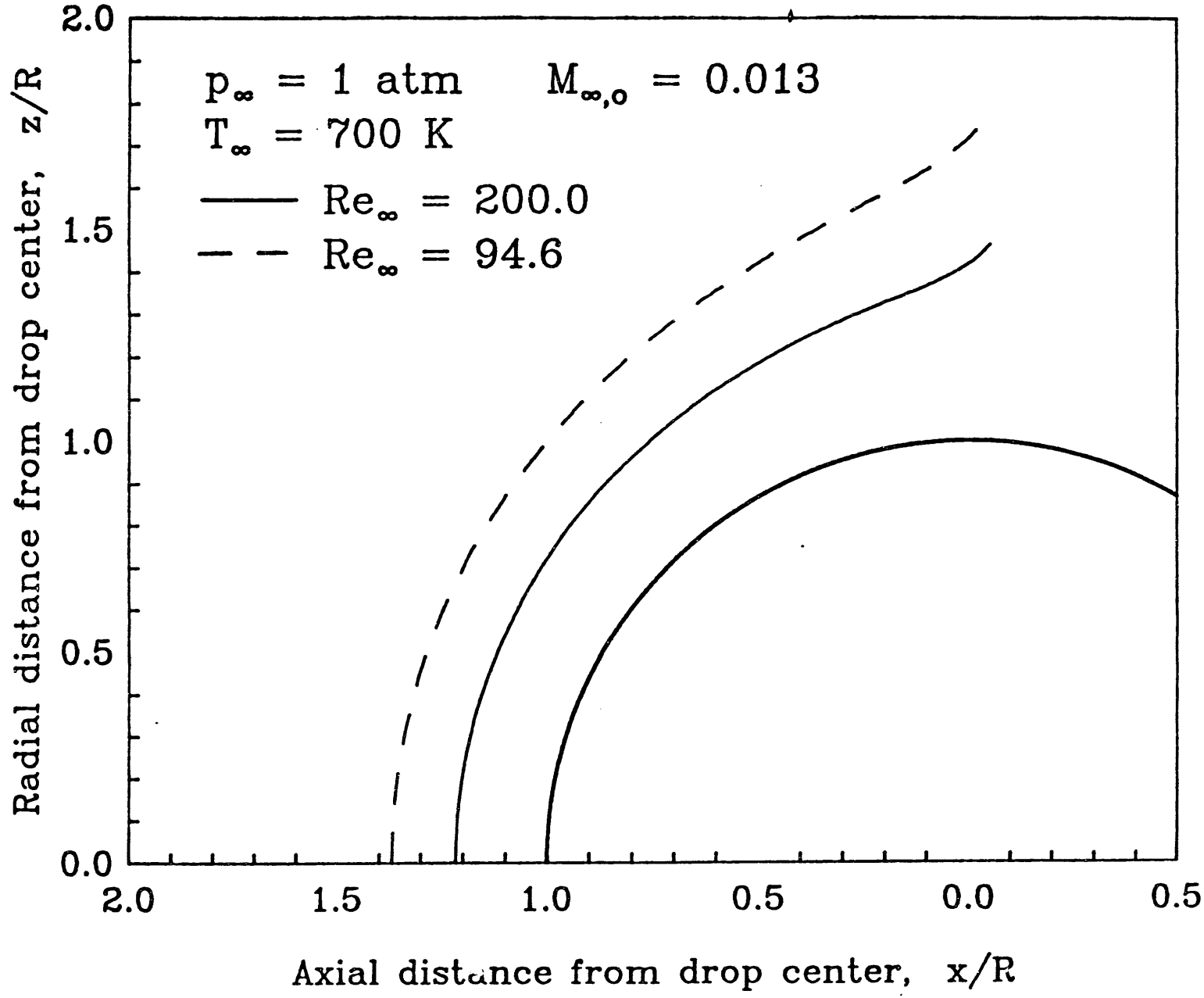

Figure 9. Predicted flame shapes about spherical droplet for two different Reynolds numbers.

END

DATE FILMED

12 / 23 / 92